Unveiling the Origin of Charge Transport in $SrTiO_3$ Beyond the Quasiparticle Regime

Jin-Jian Zhou[1] and Marco Bernardi[1,*]

[1]*Department of Applied Physics and Materials Science, California Institute of Technology, Pasadena, CA 91125, USA.*

(Dated: May 10, 2019)

In materials with strong electron-phonon (e-ph) interactions, the electrons carry a phonon cloud during their motion, forming quasiparticles known as polarons. Charge transport and its temperature dependence in the polaron regime remain poorly understood. Here, we present first-principles calculations of charge transport in a prototypical material with large polarons, $SrTiO_3$. Using a cumulant diagram-resummation technique that can capture the strong e-ph interactions, our calculations can accurately predict the experimental electron mobility in $SrTiO_3$ between 150−300 K. They further reveal that for increasing temperature the charge transport mechanism transitions from band-like conduction, in which the scattering of renormalized quasiparticles is dominant, to an incoherent transport regime governed by dynamical interactions between the electrons and their phonon cloud. Our work reveals long-sought microscopic details of charge transport in $SrTiO_3$, and provides a broadly applicable method for predicting charge transport in materials with strong e-ph interactions and polarons.

Understanding charge transport in complex materials is a grand challenge of fundamental and technological relevance. The interactions between electrons and phonons (the quanta of lattice vibrations) set an intrinsic limit for the conductivity and typically control charge transport near room temperature. When electron-phonon (e-ph) interactions are weak, charge transport is well described by the scattering of quasiparticles (QPs) [1], leading to the well-known band-like conduction regime. As the e-ph interactions become stronger, the electrons are dressed by a cloud of phonons, forming composite charge carriers known as polarons [2–4]. In the limit of strong e-ph coupling, the electrons are self-trapped by the lattice distortions, and the conduction mechanism becomes the thermally activated hopping of localized polarons [5].

Many oxides and organic crystals exhibit e-ph coupling strengths intermediate between the band-like and polaron hopping limits. In this so-called "large polaron" regime, the charge transport mechanisms and their temperature dependence are not well understood. The transition from band-like to hopping conduction for increasing e-ph coupling strength is also unclear, though recent work on the Holstein model uncovered an incoherent transport regime at intermediate coupling [6]. Yet, predictive calculations and microscopic understanding of charge transport in the intermediate e-ph coupling regime remain an open challenge.

Strontium titanate ($SrTiO_3$), which is stable in the cubic phase above 105 K, is a prototypical material with intermediate e-ph coupling in which large polaron effects are clearly seen in experiments [7–10]. Charge transport in $SrTiO_3$ is a decades-old problem [11–16], yet its underlying microscopic mechanisms are still debated [17]. The electron mobility in cubic $SrTiO_3$ exhibits a roughly T^{-3} temperature dependence above 150 K [15, 16], which is commonly attributed to the scattering of electron QPs with phonons [11–14]. Different phenomenological models based on QP scattering have been proposed that can fit the experimental transport data [13, 18]. However, the carrier mean free paths extracted from experiment in $SrTiO_3$ fall below the interatomic distance [16], violating the Mott-Ioffe-Regel (MIR) criterion for the applicability of the QP scattering picture [19].

First-principles calculations based on lowest-order e-ph scattering plus the Boltzmann transport equation (BTE) [20] can accurately predict the conductivity in simple metals and semiconductors [21–25]. We have recently shown [26] that when this approach is applied to $SrTiO_3$, one can obtain an accurate temperature dependence for the electron mobility if all the phonons (including the soft modes) are taken into account. However, the absolute value of the computed electron mobility is an order of magnitude greater than experiment [26]. It is clear that QP scattering alone cannot explain charge transport in $SrTiO_3$, consistent with the MIR limit violation.

Here, we show first-principles calculations of charge transport in cubic $SrTiO_3$ using a finite-temperature retarded cumulant approach that includes higher-order e-ph interactions and goes beyond the QP scattering picture. Our calculations can accurately predict the experimental electron mobility in $SrTiO_3$ between 150−300 K, and further shed light on its microscopic origin. We show that the weight of the QP peak in the electron spectral function is strongly renormalized, with significant weight transfer to the incoherent phonon satellites. While the renormalized QPs control transport at low temperature, the incoherent contributions from the phonon satellites and large momentum states are significant at room temperature, indicating a transport regime beyond the QP scattering paradigm. Our work opens new avenues for computing charge transport beyond the QP scattering regime in complex materials with large polarons.

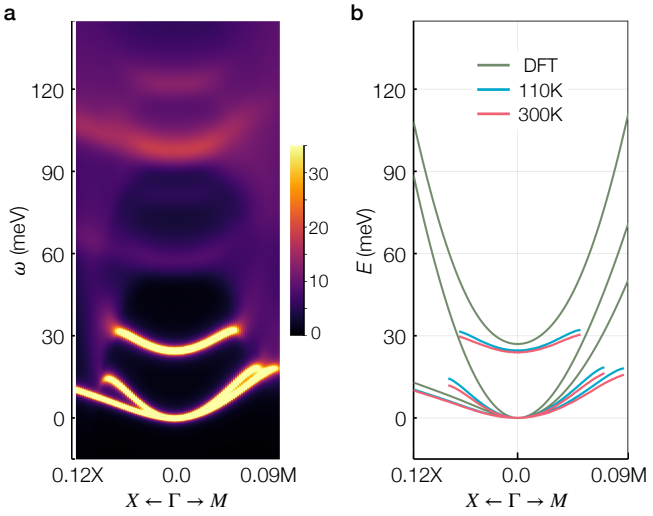

FIG. 1. (a) Combined spectral functions $A_{n\boldsymbol{k}}(\omega)$ for the three lowest conduction bands in cubic $SrTiO_3$, for $\boldsymbol{k}$ along the $\Gamma-X$ and $\Gamma-M$ Brillouin zone directions at 110 K. (b) The energy-momentum dispersion of the QP peaks of the spectral function, shown at 110 K and 300 K, compared with the electronic band structure from DFT. The zero of the energy axis is set to the conduction band minimum.

Electron spectral function

Central to our approach for computing charge transport is the electron spectral function, $A(\omega)$, which can be seen as the density of states of a single electron. Due to the interactions with the phonons, the spectral function consists of a QP peak representing a single-electron-like excitation and an incoherent part including both phonon satellite peaks and a background contribution [27, 28]. While the spectral weights of the QP peak and incoherent part may vary, they always add up to one due to the sum rule $\int d\omega A(\omega) = 1$, which amounts to a conservation of the electron. To investigate the dynamics of the electrons and their interactions with the phonons, we compute the spectral function with a finite-temperature retarded cumulant approach that can account for higher-order e-ph interactions, and use it directly to predict transport, without relying on QP scattering approaches.

We focus on the electron spectral function in cubic $SrTiO_3$ above 110 K. Leveraging our recently developed scheme [26], which combines density functional theory (DFT), its linear response extension [29] and the temperature dependent effective potential (TDEP) method [30], we compute the band structure, lattice vibrations and e-ph interactions for all phonon modes, including the soft modes due to the lattice anharmonicity (see Methods). Using these quantities, we calculate the spectral function using a retarded cumulant formalism [31, 32]. In this framework, the e-ph interactions for each electronic state with band index n and momentum $\boldsymbol{k}$ are included in the one-particle retarded Green's function $G^R_{n\boldsymbol{k}}$ via the so-called cumulant function $C_{n\boldsymbol{k}}(t)$:

$$G^R_{n\boldsymbol{k}}(\omega) = -i\int_0^\infty e^{i(\omega-\varepsilon_{n\boldsymbol{k}})t} e^{C_{n\boldsymbol{k}}(t)} dt \ , \qquad (1)$$

where $\varepsilon_{n\boldsymbol{k}}$ is the DFT band electron energy and $C_{n\boldsymbol{k}}(t)$ is obtained from the off-shell lowest-order e-ph self-energy, $\Sigma_{n\boldsymbol{k}}(\omega)$ [20], as

$$C_{n\boldsymbol{k}}(t) = \int_{-\infty}^{\infty} d\omega \frac{|\mathrm{Im}\Sigma_{n\boldsymbol{k}}(\omega+\varepsilon_{n\boldsymbol{k}})|}{\pi\omega^2}\left(e^{-i\omega t} + i\omega t - 1\right). \qquad (2)$$

The spectral function is then obtained from the retarded Green's function, using $A_{n\boldsymbol{k}}(\omega) = -\mathrm{Im}G^R_{n\boldsymbol{k}}(\omega)/\pi$. The cumulant approach includes higher-order e-ph Feynman diagrams beyond the Migdal approximation [33], thus producing accurate spectral functions [34] that can capture the strong e-ph interactions. Our finite-temperature extension of the retarded cumulant approach (see Methods) further allows us to compute the spectral function at different temperatures.

The computed electron spectral functions for the three lowest conduction bands in cubic $SrTiO_3$ at 110 K are combined in a color map and shown in Fig. 1a. Each state exhibits a rather sharp QP peak at low energy and broader phonon satellite peaks at higher energies (∼60 meV or more above the QP peak). By tracking the low-energy QP peaks, we map the energy-momentum dispersion of the QPs. Figure 1b shows that the interacting QPs exhibit a heavier effective mass than in the DFT band structure calculations, in which the e-ph interactions are not included. The mass enhancement is a factor of 1.8−2.6 for different bands and directions, and it increases only slightly with temperature. Taking the lowest bands along Γ−M as an example, the DFT effective mass is roughly $0.75m_e$ (m_e is the electron mass), compared to a QP effective mass of $1.4m_e$ at 110 K and a slightly heavier mass of $1.6m_e$ at 300 K. The mass enhancement is thus roughly a factor of 2, in excellent agreement with experimental results at light doping [7, 10].

The interactions with the surrounding phonons not only make the electron QPs heavier, they also significantly reduce the QP spectral weight to a value of much less than unity, transferring weight to the higher-energy incoherent phonon satellites. The QP peak even disappears at large electron momenta, leaving a spectral function made up entirely by the incoherent background. These trends are analyzed in detail below in Fig. 2, where we focus on how the spectral function of the lowest conduction band changes as a function of temperature and momentum.

The spectral function at the conduction band minimum at Γ exhibits a main QP peak, two main satellites (also known as phonon sidebands or replicas), and weaker additional satellites at higher energy (see Fig. 2a). The two main satellite peaks are at an energy $\omega_{\text{LO-1}} = 98$ meV and $\omega_{\text{LO-2}} = 57$ meV above the main QP peak; these val-

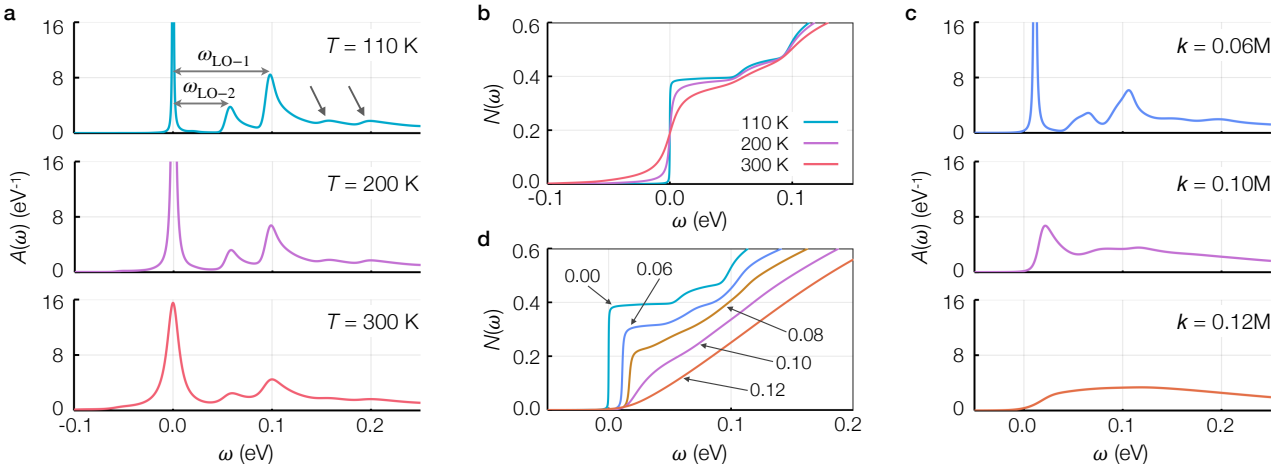

FIG. 2. Computed electron spectral functions $A_{\boldsymbol{k}}(\omega)$ for the lowest conduction band in cubic $SrTiO_3$. In each panel, the zero of the ω energy axis is set to the energy of the QP peak at the Γ point. (a) The spectral function $A_{\boldsymbol{k}}(\omega)$ at three temperatures values between 110−300 K, for $\boldsymbol{k} = \Gamma$. The energies of the two LO phonons coupling strongly with the electrons are labelled $\omega_{\text{LO-1}}$ and $\omega_{\text{LO-2}}$, and the arrows point to the second set of satellites at $2\omega_{\text{LO-1}}$ and $\omega_{\text{LO-1}} + \omega_{\text{LO-2}}$. (b) The spectral weight $N(\omega)$ obtained by integrating the spectral function up to an energy ω. (c) The spectral function $A_{\boldsymbol{k}}(\omega)$ at 110 K for different values of $\boldsymbol{k}$ along the $\Gamma-M$ Brillouin zone line, and (d) The corresponding integrated spectral weight $N(\omega)$.

ues correspond, respectively, to the energies of the two longitudinal optical (LO) modes with long-range e-ph interactions that exhibit the strongest coupling with electrons [26]. The main phonon sidebands are associated with the polaron plus one-phonon continuum, and are a hallmark of the large polaron regime [35]. Their presence in cubic $SrTiO_3$ is consistent with recent ARPES measurements [9, 10], which revealed a phonon sideband for holes roughly ∼100 meV away from the QP peak. Note also the presence in Fig. 2a of weak phonon sideband peaks at energies of $2\omega_{\text{LO-1}}$ and $\omega_{\text{LO-1}} + \omega_{\text{LO-2}}$. These higher-order replicas, which are known to occur in the strong coupling limit of the Holstein model [36], are akin to the higher harmonics observed in phonon Floquet states [37]; they are a signature of strong coupling with the LO modes.

To compute the spectral weights of the QP peak and incoherent part, we integrate the spectral function up to an energy ω, obtaining the spectral weight $N(\omega) = \int_{-\infty}^{\omega} A(\omega')d\omega'$ given in Fig. 2b. We find that the spectral weight of the QP peak is ∼0.4 at 110 K, and thus much less than its unit value in the weak e-ph interaction limit. As the temperature increases from 110 K to 300 K, both the QP peak and the phonon satellites are broadened and smeared out, but the QP spectral weight changes only slightly, primarily due to an overlap between the QP peak and the phonon satellites near 300 K. We conclude that at all temperatures between 110−300 K, the QP weight is strongly renormalized to a value of ∼0.4. Pictorially, only half of the electron resides in the QP state, while the other half contributes to the incoherent dynamical interactions with the phonon cloud.

Figure 2c reveals the disappearance of the QP peak at large enough momentum $\boldsymbol{k}$ by showing how the spectral function changes as we increase $\boldsymbol{k}$ along the $\Gamma-M$ Brillouin zone line. We find that the QP spectral weight decreases with increasing momentum (see Fig. 2d); the QP peak ultimately disappears at $\boldsymbol{k} = 0.12M$, leading to a fully incoherent spectral function at larger momenta. These so-called end points of the QP peak, which have been predicted in both the Fröhlich [38] and Holstein models [39], are yet another signature of the strong e-ph interactions. The decrease of the QP spectral weight and the disappearance of the QP peak at large momentum have a significant impact on transport, as we show below.

Electron mobility and its microscopic origin

Large polaron transport is commonly believed to be the band-like conduction of QPs with enhanced effective mass. However, this simplified picture neglects the fact that the QP weight can drop to values much smaller than one (here, to roughly 0.4, as we saw above), and that the contribution to transport from the incoherent part of the spectral function can be significant. Temperature also plays a primary role. At low temperature, the electrons occupy the low-energy QP states, and there are only few LO phonons due to their relatively high energy. As the temperature increases, thermal fluctuations push the electrons to higher energies, exciting the electrons outside of the QP peak into the incoherent regime. In addition, the number of LO phonons grows rapidly with temperature, leading to strong dynamical interactions between the electron and its phonon cloud. The incoherent contributions are thus expected to significantly influence transport at higher temperatures.

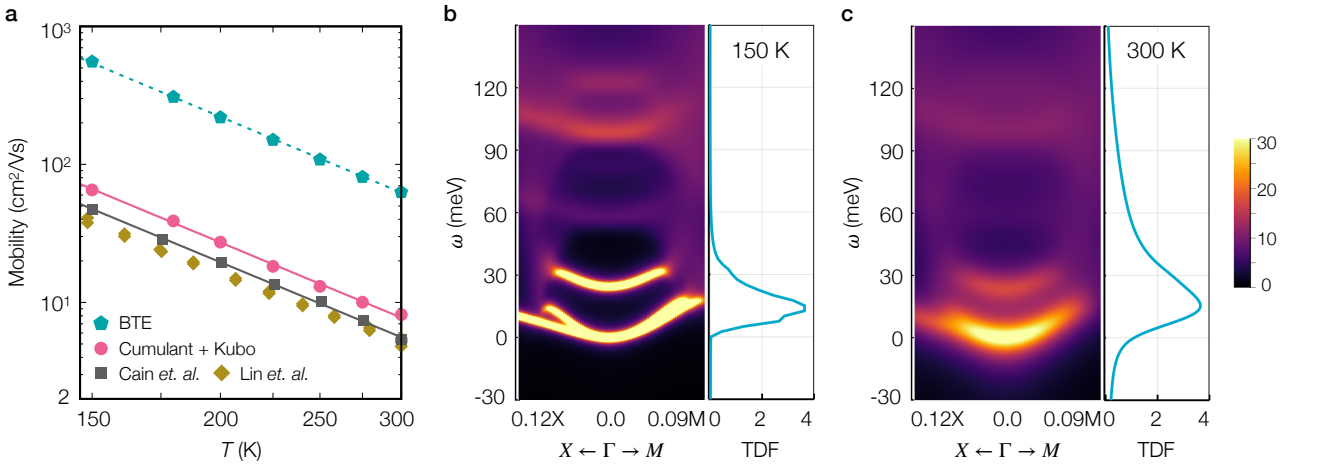

FIG. 3. (a) Electron mobility as a function of temperature, computed using the retarded cumulant approach plus the Kubo formula (red circles) and compared with experimental values taken from Refs. [15, 16]. The mobility computed in Ref. [26] using lowest-order e-ph interactions plus the BTE is also shown (blue pentagons). (b) The combined conduction-band spectral functions at $T = 150$ K are shown together with the TDF defined in Eq. 4, which quantifies the contribution to the DC conductivity as a function of electron energy ω. (c) The same quantities as in (b) shown at $T = 300$ K. The zero of the energy axis is set to the energy of the lowest QP peak.

To investigate these points quantitatively in $SrTiO_3$, we compute the conductivity directly from the spectral functions – therefore including both the QP and incoherent contributions – using the Kubo formula [35, 40]:

$$\sigma_{\alpha\beta}(\omega) = \frac{\pi\hbar e^2}{V_{\rm uc}} \int d\omega' \frac{f(\omega') - f(\omega'+\omega)}{\omega} \times \sum_{n\boldsymbol{k}} v^{\alpha}_{n\boldsymbol{k}}\, v^{\beta}_{n\boldsymbol{k}}\, A_{n\boldsymbol{k}}(\omega')\, A_{n\boldsymbol{k}}(\omega'+\omega)\ , \tag{3}$$

where $\boldsymbol{v}_{n\boldsymbol{k}}$ is the electron band velocity, $f(\omega)$ is the Fermi-Dirac distribution, $V_{\rm uc}$ is the unit cell volume, and α and β are Cartesian directions. We also compute the DC conductivity, using $\sigma^{dc} = \sigma(\omega \to 0)$, and the electron mobility as $\mu = \sigma^{dc}/n_c e$, where n_c is the carrier concentration (see Methods). Note that in the weak e-ph coupling limit, in which the spectral function consists only of a sharp QP peak with unit weight, the expression we use for σ^{dc} reduces to the conductivity obtained from the relaxation time approximation of the BTE [40].

Our computed electron mobility as a function of temperature is shown in Fig. 3a and compared with experimental data taken from Refs. [15, 16]. Both the temperature dependence and the absolute value of the computed mobility are in excellent agreement with experiments. Our computed mobility at 300 K is about 8 $\rm cm^2/V\,s$, versus an experimental value of ∼5 $\rm cm^2/V\,s$ [15, 16]. For comparison, the mobility obtained using lowest-order e-ph interactions plus the BTE is an order of magnitude higher than experiments [26], as also shown in Fig. 3a. Note that both the BTE and the cumulant calculations can accurately predict the temperature dependence of the mobility, mainly because they both use accurate phonon dispersions and e-ph interactions for all the phonons, including the soft modes [26].

The order-of-magnitude mobility drop from the lowest-order e-ph theory to the cumulant approach is due to both the QP renormalization and the incoherent contributions. Our results show that including higher-order e-ph processes and incoherent polaron effects via the cumulant approach greatly improves the computed mobility over the established lowest-order e-ph plus BTE approach [20–25]. These results also show that the lowest-order first-principles approach is accurate only in the limit of weak e-ph interactions.

Our approach to computing the conductivity further allows us to resolve the coherent and incoherent contributions to transport and to uncover different transport regimes as a function of temperature. The integrand in the DC conductivity formula (see Methods),

$$\Phi(\omega) = -\frac{\partial f(\omega)}{\partial\omega} \sum_{n\boldsymbol{k}} v^{\alpha}_{n\boldsymbol{k}}\, v^{\beta}_{n\boldsymbol{k}}\, |A(n\boldsymbol{k},\omega)|^2\,, \tag{4}$$

is referred to as the transport distribution function (TDF), and is employed here to quantify the contributions to the DC conductivity as a function of electron energy ω. We analyze the TDF in the 150−300 K range in Fig. 3b,c, and find that both the coherent QP peak and the incoherent part contribute to transport. At temperatures below ∼200 K, the TDF spans primarily the QP peaks (see Fig. 3b), implying that transport is dominated by the scattering of QPs with a strongly renormalized spectral weight. As the temperature increases, the high-energy tail of the TDF extends over the incoherent contributions (see Fig. 3c), which become important. Near room temperature, transport is governed not only by the weight-renormalized QPs, but also by the inco-

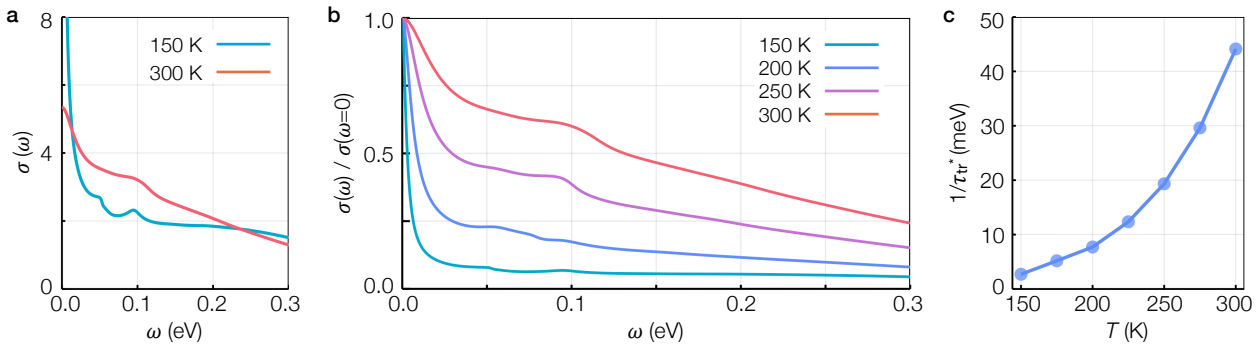

FIG. 4. (a) Comparison between the computed optical conductivities at 150 K and 300 K. The curves were normalized to possess the same integral. (b) Computed optical conductivity divided by the DC conductivity at each temperature. (c) The inverse of the effective transport relaxation time, $\tau^{*\,-1}_{\rm tr}$, extracted from $\sigma(\omega)$ and shown as a function of temperature.

herent phonon satellites above the QP peaks and by the polaron states at large momenta beyond the end points, where the QP peaks disappear. Therefore, the picture of QP scattering is inadequate to describe transport at room temperature in $SrTiO_3$. A more complex picture emerges in which transport is an interplay between the QP renormalization and the contributions from the incoherent phonon sidebands and from the polaron states beyond the end points, all of which are consequences of the dynamical interactions with the LO phonon cloud.

These conclusions are supported by experiments on the optical conductivity. Recent experiments in $SrTiO_3$ show that the Drude peak at low frequency in the optical conductivity, which is associated with the coherent band-like transport of QPs, loses weight for increasing temperatures up to 300 K [7, 8]. Figure 4a compares the low-energy optical conductivities at 150 K and 300 K, computed with Eq. 3 and normalized to possess the same integral, consistent with the optical sum rule. The optical conductivities exhibit a Drude-like peak centered at zero frequency, and an incoherent shoulder structure consisting of phonon sidebands plus a broad background. We find a significant weight transfer from the Drude peak to the incoherent shoulder as the temperature increases from 150 K to 300 K, in agreement with experiments [7]. The Drude peak is sharp at 150 K, but it broadens rapidly as the temperature increases (see Fig. 4b). These trends confirm the transition seen in our transport results from a renormalized QP regime at low temperature to an incoherent, beyond-QP regime near room temperature.

We extract an effective transport relaxation time, $\tau^*_{\rm tr}$, from the optical conductivity through the extended Drude analysis of Ref. [41]:

$$\tau^*_{\rm tr} = -\frac{2}{\pi\sigma^{dc}}\int_0^\infty \frac{1}{\omega'}\frac{\partial\sigma(\omega')}{\partial\omega'}d\omega'. \qquad (5)$$

Figure 4c shows the inverse of $\tau^*_{\rm tr}$, namely the effective scattering rate characterizing the width of the Drude peak. We find that this effective scattering rate increases rapidly with temperature, reaching values much greater than the QP scattering rate extracted from the QP peak of the spectral function in Fig. 2a. Surprisingly, the scattering time exceeds the Planckian limit k_BT at 300 K [42], highlighting the incoherent nature of charge transport in $SrTiO_3$ near room temperature.

In summary, we developed a broadly applicable approach for computing charge transport in the large polaron regime in materials with intermediate e-ph coupling strenght. Our calculations on $SrTiO_3$ unveil a transition from band-like transport of strongly weight-renormalized QPs at low temperature to an incoherent transport regime beyond the QP picture near room temperature. Our approach can shed new light on broad classes of materials with polaron effects, ranging from perovskites [43] and transition metal oxides [44, 45] to high-Tc superconductors [46, 47].

J.-J.Z. has benefited from discussion with N.-E. Lee. This work was supported by the Joint Center for Artificial Photosynthesis, a DOE Energy Innovation Hub, supported through the Office of Science of the U.S. Department of Energy under Award No. DE-SC0004993. M.B. acknowledges support by the National Science Foundation under Grant No. ACI-1642443, which provided for code development, and Grant No. CAREER-1750613, which provided for theory and method development. This work was partially supported by the Air Force Office of Scientific Research through the Young Investigator Program, Grant FA9550-18-1-0280. This research used resources of the National Energy Research Scientific Computing Center, a DOE Office of Science User Facility supported by the Office of Science of the U.S. Department of Energy under Contract No. DE-AC02-05CH11231.

* E-mail: bmarco@caltech.edu

[1] Ziman, J. M. *Electrons and Phonons: The Theory of Transport Phenomena in Solids* (Oxford University Press, New York, 2007).

[2] Frhlich, H. Electrons in lattice fields. *Adv. Phys.* **3**, 325–361 (1954).

[3] Holstein, T. Studies of polaron motion. *Ann. Phys.* **8**, 343–389 (1959).

[4] Devreese, J. T. & Alexandrov, A. S. Frhlich polaron and bipolaron: recent developments. *Rep. Prog. Phys.* **72**, 066501 (2009).

[5] Emin, D. *Polarons* (Cambridge University Press, 2012).

[6] Mishchenko, A., Nagaosa, N., De Filippis, G., de Candia, A. & Cataudella, V. Mobility of Holstein polaron at finite temperature: An unbiased approach. *Phys. Rev. Lett.* **114**, 146401 (2015).

[7] van Mechelen, J. L. M. *et al.* Electron-phonon interaction and charge carrier mass enhancement in $SrTiO_3$. *Phys. Rev. Lett.* **100**, 226403 (2008).

[8] Devreese, J. T., Klimin, S. N., van Mechelen, J. L. M. & van der Marel, D. Many-body large polaron optical conductivity in $SrTi_{1-x}Nb_xO_3$. *Phys. Rev. B* **81**, 125119 (2010).

[9] Chen, C., Avila, J., Frantzeskakis, E., Levy, A. & Asensio, M. C. Observation of a two-dimensional liquid of Frhlich polarons at the bare $SrTiO_3$ surface. *Nat. Commun.* **6**, 9585 (2015).

[10] Wang, Z. *et al.* Tailoring the nature and strength of electronphonon interactions in the $SrTiO_3$(001) 2d electron liquid. *Nat. Mater.* **15**, 835–839 (2016).

[11] Frederikse, H. P. R. & Hosler, W. R. Hall mobility in $SrTiO_3$. *Phys. Rev.* **161**, 822–827 (1967).

[12] Wemple, S. H., DiDomenico, M. & Jayaraman, A. Electron scattering in perovskite-oxide ferroelectric semiconductors. *Phys. Rev.* **180**, 547–556 (1969).

[13] Verma, A., Kajdos, A. P., Cain, T. A., Stemmer, S. & Jena, D. Intrinsic mobility limiting mechanisms in lanthanum-doped strontium titanate. *Phys. Rev. Lett.* **112**, 216601 (2014).

[14] Zhou, W. X. *et al.* Electron−soft phonon scattering in *n*-type $SrTiO_3$. *Phys. Rev. B* **94**, 195122 (2016).

[15] Cain, T. A., Kajdos, A. P. & Stemmer, S. La-doped $SrTiO_3$ films with large cryogenic thermoelectric power factors. *Appl. Phys. Lett.* **102**, 182101 (2013).

[16] Lin, X. *et al.* Metallicity without quasi-particles in room-temperature strontium titanate. *npj Quantum Mater.* **2**, 41 (2017).

[17] Collignon, C., Lin, X., Rischau, C. W., Fauqu, B. & Behnia, K. Metallicity and superconductivity in doped strontium titanate. *Annu. Rev. Condens. Matter Phys.* **10**, 25–44 (2019).

[18] Mikheev, E. *et al.* Limitations to the room temperature mobility of two- and three-dimensional electron liquids in $SrTiO_3$. *Appl. Phys. Lett.* **106**, 062102 (2015).

[19] Hussey, N. E., Takenaka, K. & Takagi, H. Universality of the MottIoffeRegel limit in metals. *Philos. Mag.* **84**, 2847–2864 (2004).

[20] Bernardi, M. First-principles dynamics of electrons and phonons. *Eur. Phys. J. B* **89**, 239 (2016).

[21] Mustafa, J. I., Bernardi, M., Neaton, J. B. & Louie, S. G. *Ab initio* electronic relaxation times and transport in noble metals. *Phys. Rev. B* **94**, 155105 (2016).

[22] Zhou, J.-J. & Bernardi, M. *Ab initio* electron mobility and polar phonon scattering in GaAs. *Phys. Rev. B* **94**, 201201 (2016).

[23] Liu, T.-H., Zhou, J., Liao, B., Singh, D. J. & Chen, G. First-principles mode-by-mode analysis for electron-phonon scattering channels and mean free path spectra in GaAs. *Phys. Rev. B* **95**, 075206 (2017).

[24] Ma, J., Nissimagoudar, A. S. & Li, W. First-principles study of electron and hole mobilities of Si and GaAs. *Phys. Rev. B* **97**, 045201 (2018).

[25] Lee, N.-E., Zhou, J.-J., Agapito, L. A. & Bernardi, M. Charge transport in organic molecular semiconductors from first principles: The bandlike hole mobility in a naphthalene crystal. *Phys. Rev. B* **97**, 115203 (2018).

[26] Zhou, J.-J., Hellman, O. & Bernardi, M. Electron-phonon scattering in the presence of soft modes and electron mobility in $SrTiO_3$ perovskite from first principles. *Phys. Rev. Lett.* **121**, 226603 (2018).

[27] Damascelli, A., Hussain, Z. & Shen, Z.-X. Angle-resolved photoemission studies of the cuprate superconductors. *Rev. Mod. Phys.* **75**, 473–541 (2003).

[28] Martin, R. M., Reining, L. & Ceperley, D. M. *Interacting Electrons: Theory and Computational Approaches* (Cambridge University Press, 2016).

[29] Baroni, S., de Gironcoli, S., Dal Corso, A. & Giannozzi, P. Phonons and related crystal properties from density-functional perturbation theory. *Rev. Mod. Phys.* **73**, 515–562 (2001).

[30] Hellman, O., Abrikosov, I. A. & Simak, S. I. Lattice dynamics of anharmonic solids from first principles. *Phys. Rev. B* **84**, 180301 (2011).

[31] Kas, J. J., Rehr, J. J. & Reining, L. Cumulant expansion of the retarded one-electron Green function. *Phys. Rev. B* **90**, 085112 (2014).

[32] Kas, J. & Rehr, J. Finite temperature Green's function approach for excited state and thermodynamic properties of cool to warm dense matter. *Phys. Rev. Lett.* **119**, 176403 (2017).

[33] Hedin, L. On correlation effects in electron spectroscopies and the GW approximation. *J. Phys.: Condens. Matter* **11**, R489 (1999).

[34] Nery, J. P. *et al.* Quasiparticles and phonon satellites in spectral functions of semiconductors and insulators: Cumulants applied to the full first-principles theory and the Fröhlich polaron. *Phys. Rev. B* **97**, 115145 (2018).

[35] Mahan, G. D. *Many-Particle Physics* (Springer US, 2000), 3rd edn.

[36] Berciu, M. Green's function of a dressed particle. *Phys. Rev. Lett.* **97**, 036402 (2006).

[37] Hübener, H., De Giovannini, U. & Rubio, A. Phonon driven floquet matter. *Nano Lett.* **18**, 1535–1542 (2018).

[38] Mishchenko, A. S., Prokofev, N. V., Sakamoto, A. & Svistunov, B. V. Diagrammatic quantum Monte Carlo study of the Fröhlich polaron. *Phys. Rev. B* **62**, 6317–6336 (2000).

[39] Goodvin, G. L. & Berciu, M. The end points in the dispersion of Holstein polarons. *Europhys. Lett.* **92**, 37006 (2010).

[40] Allen, P. B. Electron self-energy and generalized Drude formula for infrared conductivity of metals. *Phys. Rev. B* **92**, 054305 (2015).

[41] Deng, X., Sternbach, A., Haule, K., Basov, D. & Kotliar, G. Shining light on transition-metal oxides: Unveiling

the hidden fermi liquid. *Phys. Rev. Lett.* **113**, 246404 (2014).

[42] Hartnoll, S. A. Theory of universal incoherent metallic transport. *Nat. Phys.* **11**, 54–61 (2015).

[43] Miyata, K., Atallah, T. L. & Zhu, X.-Y. Lead halide perovskites: Crystal-liquid duality, phonon glass electron crystals, and large polaron formation. *Sci. Adv.* **3**, e1701469 (2017).

[44] Moser, S. *et al.* Tunable polaronic conduction in anatase TiO_2. *Phys. Rev. Lett.* **110**, 196403 (2013).

[45] Cancellieri, C. *et al.* Polaronic metal state at the $LaAlO_3/SrTiO_3$ interface. *Nat. Commun.* **7**, 10386 (2016).

[46] Lanzara, A. *et al.* Evidence for ubiquitous strong electron–phonon coupling in high-temperature superconductors. *Nature* **412**, 510 (2001).

[47] Legros, A. *et al.* Universal T-linear resistivity and planckian dissipation in overdoped cuprates. *Nat. Phys.* **15**, 142–147 (2019).